Editors' Suggestion   Featured in Physics

Nonaffine Mechanics of Entangled Networks Inspired by Intermediate Filaments

Marco Pensalfini[1,*], Tom Golde[2], Xavier Trepat[2,3,4,5] and Marino Arroyo[1,2,6,†]

[1]*Laboratori de Càlcul Numeric (LaCàN), Universitat Politècnica de Catalunya-BarcelonaTech, 08034 Barcelona, Spain*
[2]*Institute for Bioengineering of Catalonia (IBEC), The Barcelona Institute of Science and Technology (BIST), 08028 Barcelona, Spain*
[3]*Departament de Biomedicina, Facultat de Medicina, Universitat de Barcelona, 08036 Barcelona, Spain*
[4]*Institució Catalana de Recerca i Estudis Avançats (ICREA), 08010 Barcelona, Spain*
[5]*Centro de Investigación Biomédica en Red en Bioingeniería, Biomateriales y Nanomedicina (CIBER-BBN), 08028 Barcelona, Spain*
[6]*Centre Internacional de Mètodes Numèrics en Enginyeria (CIMNE), 08034 Barcelona, Spain*

Inspired by massive intermediate filament (IF) reorganization in superstretched epithelia, we examine computationally the principles controlling the mechanics of a set of entangled filaments whose ends slide on the cell boundary. We identify an entanglement metric and threshold beyond which random loose networks respond nonaffinely and nonlinearly to stretch by self-organizing into structurally optimal star-shaped configurations. A simple model connecting cellular and filament strains links emergent mechanics to cell geometry, network topology, and filament mechanics. We identify a safety net mechanism in IF networks and provide a framework to harness entanglement in soft fibrous materials.

Epithelial tissues are cohesive cellular sheets lining free surfaces in multicellular eukaryotes. They are involved in crucial physiological processes such as morphogenesis, protection, secretion, and absorption [1–4]. Being biological barriers, they need to preserve integrity within active and challenging mechanical environments. Depending on the temporal scales and system, epithelial mechanics may depend on cellular rearrangements or on deformation of individual cells, which in turn depends on intracellular cytoskeletal networks that are mechanically integrated at the tissue scale through cell-cell junctions [5–8]. These cytoskeletal networks are composite systems combining widely diverse biopolymers, which interact chemically, physically, and through biological regulation [9–12].

Cytoskeletal actin filaments are short (< 1 μm [13]), stiff both to stretch and bending [9,14,15], bind to a variety of specific cross-linkers including myosin motors, and turn over within minutes [9]. Microtubules are long, stiff, dynamic, and also bind to specific motors. Conversely, intermediate filaments (IFs) organize into long (several micrometers [16]), bendable [9,15], and highly stretchable bundles, with a highly nonlinear force-stretch behavior enabling extensions of up to 3–4.5-fold [17–22]. IF turnover is much slower [9,23], in the order of hours, and unlike other cytoskeletal filaments, they lack stable and specific linkers, although unspecific cytolinkers such as

plectin bind IFs to other IFs including nuclear lamins, to actin, or to microtubules [24]. IFs form supracellular networks thanks to adhesion complexes known as desmosomes [6]. Together, these features support the view that IFs form a relatively passive network providing a "safety belt" against fast and large deformations [19,21,25–27], although how load is transferred from the tissue scale to individual IFs remains poorly understood.

Recent stretching experiments on epithelial monolayers suggest synergistic interactions between the actin cytoskeleton, controlling epithelial mechanics at moderate stretches, and IFs, providing load bearing under very large cell deformations [4,7,23,28]. Under extreme cellular stretches and over long times, the IF network rearranges
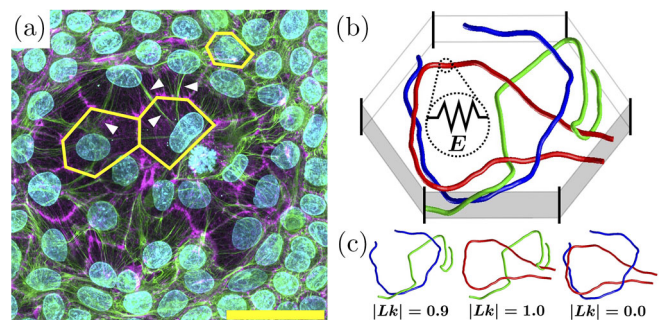
FIG. 1. (a) Superstretched cells in an epithelial dome [4] with radial IF bundles (white arrowheads; green, keratin 18 IFs; magenta, actin; cyan, nuclei; scale bar, 40 μm), where yellow polygons mark selected cell outlines. (b) Sketch of a discrete network model of IFs in a cell with elastic, bendable filaments whose ends slide on the cell boundary. (c) Illustration of the pairwise Gaussian linking number for the filaments in (b).

into a characteristic "star-shaped" structure where thick bundles radiate from a central tight tangle, Fig. 1(a) [4]. Laser ablation shows that such IF bundles provide structural integrity to superstretched cells as the actin network becomes progressively diluted. Since IFs appear wavy and cortically arranged in unloaded cells, we wondered about the physical mechanisms underlying this slack-taut transition and the corresponding effects on network-scale mechanics.

To address these questions, we focused on the mechanics of IF networks alone. Although actin or nuclear lamins may limit the reconfigurations of the IF network by entanglements and cross-links, the separation of turnover timescales mentioned earlier justifies a slow loading regime in which these constraints have time to relax, but entanglements between IFs and their binding to desmosomes remain intact. Given the extreme extensibility of IFs [17–22,29], we ignore filament damage. We thus idealize the IF cytoskeleton within a cell as a loose and entangled network of un-cross-linked, bendable, and extensible filaments, whose ends are attached to the lateral boundaries of a prismatic domain, Fig. 1(b). These idealized desmosomes prevent unraveling of the network by filament reptation. Since the IF network is corralled into cellular compartments, we regard this cell as a minimal mechanical unit [yellow hexagons in Fig. 1(a)].

We modeled such networks using the cytoskeletal simulation suite CYTOSIM [30,31] for the Brownian dynamics of inextensible and bendable filaments, which we customized to model extensible filaments with general constitutive relations [32]. We prepared computational models comprising N_f cylindrical filaments of persistence length ℓ_p, reference length $\ell_0 \gg \ell_p$, and diameter $\phi \ll \ell_0$, according to the procedure described in Sec. S1 in the Supplemental Material [33]. We initially considered linearly elastic filaments with modulus E. All filament points are confined inside the cell volume, interact sterically to avoid mutual crossing, and are subjected to a drag force with coefficient ν, Sec. S7 in [33]. We modeled the cell as a right regular prism whose base has N_e edges, apothem length a_0, surface area A_0, and side length $s_0 = 2a_0 \tan(\pi/N_e)$; the prism height is $h_0 = a_0/4$. The model parameters and their rationale are provided in Table S2 and Sec. S2 in [33], although our main results are rather insensitive to material parameters.

To simulate the extreme equibiaxial stretching reached by individual cells in pressurized lumens *in vitro* [4] and in developing embryos [41], we gradually increased the cell area A by 11-fold at a slow strain rate, much smaller than the inverse intrinsic time constant of the system E/ν. During stretching, filament ends remain attached to the lateral boundaries such that the attachment locations may move laterally within a face but not to neighboring faces, in agreement with the notion that desmosomes can move laterally in adhered pairs of plasma membranes but cannot

cross tricellular junctions. As we change A, and hence the areal strain, $\varepsilon_c = A/A_0 - 1$, we quantify the forces acting on the side walls. If $\boldsymbol{F}_i^+$ and $\boldsymbol{F}_i^-$ are the forces on the ith filament ends, and $\hat{\boldsymbol{n}}_i^+$ and $\hat{\boldsymbol{n}}_i^-$ are the normals to the walls that constrain those ends, the total force is $F_c = \sum_{i=1}^{N_f}(\boldsymbol{F}_i^+ \cdot \hat{\boldsymbol{n}}_i^+ + \boldsymbol{F}_i^- \cdot \hat{\boldsymbol{n}}_i^-)$, from which we define the nominal cellular tension, $T_c = F_c/N_e s_0$, and its dimensionless equivalent $T_c^* = F_c a_0/EA_f N_e s_0$.

Lacking cross-linkers, entanglement is the only mechanism for our idealized networks to develop mechanical resistance. Thus, we established a system preparation protocol allowing us to control network entanglement by modifying the fraction of time during which filaments grow unconstrained or with their ends fixed to cell walls, Sec. S1 and Video S1 in [33]. In agreement with our rationale, a loose and randomly organized network with default parameters and strong entanglement undergoes a dramatic spontaneous reorganization when stretched, Video S2, leading to a central tight tangle from which filament bundles radiate perpendicularly to the lateral cell boundaries. The formation of such star-shaped configuration, reminiscent of IFs in superstretched epithelial cells, involves significant lateral motion of the attachment points and results in all filaments carrying load. Conversely, an equivalent system with low entanglement develops less predictable and directed network reorganizations, where only a small fraction of filaments become taut under stretch, Video S3.

The study of how entanglements restrict configurational entropy and hence the elastic properties of bulk polymeric materials has a long history [42–45]. Here instead, we sought to characterize the topological conditions for the self-organization of corralled entangled networks into star-shaped states under finite stretch. To define a predictive entanglement metric, we resorted to topological invariants, which mathematically characterize knots (embeddings of the unit circle in $\mathbb{R}^3$) and links (collection of knots) [46,47] and have been used to describe the topology of proteins and DNA [48–50]. The pairwise Gaussian linking number $Lk_{i,j}$ characterizes the number of times that a closed and oriented spatial curve δ_i winds around another oriented curve δ_j and can be computed as [46,51]

$$Lk_{i,j} = \frac{1}{4\pi}\int_0^{2\pi}\int_0^{2\pi}\frac{\mathbf{r_i}(t_i) - \mathbf{r_j}(t_j)}{|\mathbf{r_i}(t_i) - \mathbf{r_j}(t_j)|^3}\cdot[\mathbf{r_i'}(t_i) \times \mathbf{r_j'}(t_j)]dt_i dt_j,$$

(1)

where $\mathbf{r_i}(t)$ and $\mathbf{r_j}(t)$ with $t \in [0, 2\pi)$ are parametrizations of δ_i and δ_j, and the prime denotes differentiation with respect to t. For links, $Lk_{i,j}$ is an integer and is invariant with respect to deformations respecting mutual filament avoidance. For pairs of open curves with fixed ends, called tangles [46,47], $Lk_{i,j}$ is not a strict invariant, but it is still suitable to characterize pairwise linking [49], see Fig. 1(c) and Supplemental Material, Sec. S3 [33].

To fully characterize topology in networks containing many filaments, one should resort to multibody invariants beyond the pairwise Gaussian linking number. Classical work in polymer physics avoids this full enumeration and instead simplifies the topological description using two-body invariants only [42–44]. Accordingly, we considered the *total* pairwise Gaussian linking number of the network, $Lks = \sum_{j>i} |Lk_{i,j}|$, previously adopted for textiles [52]. However, neither this entanglement metric nor the *average* pairwise Gaussian linking number *per number of filaments*, Lks/N_f, predict whether a network is sufficiently entangled to self-organize into a star-shaped organization under stretch independent of the number of filaments N_f, Sec. S4 in [33]. Instead, we found that the average pairwise Gaussian linking number *per number of filament pairs*,

$$\mathcal{E} = \frac{Lks}{N_p} = \frac{2}{N_f(N_f - 1)} \sum_{j>i} |Lk_{i,j}|, \qquad (2)$$

systematically discerns between the two network behaviors illustrated in Videos S2 and S3, Sec. S4 in [33]. While $\mathcal{E}$ is not a strict topological invariant, we verified that it is essentially independent of network deformation, Sec. S5 in [33].

We then systematically examined the role of entanglement on the network mechanics by considering filament ensembles with varying degree of entanglement $\mathcal{E}$ and otherwise identical model parameters. For insufficiently entangled systems ($\mathcal{E} \lesssim 0.3$), the networks do not exhibit coherent reorganization (Videos S3 and S4 [33]), and concomitantly, the buildup of tension is insignificant [cyan and green curves in Fig. 2(a)] in line with previous findings on nonwoven textiles [53]. Since modest levels of $\mathcal{E}$ correspond to limited mutual winding, IFs not directly bridging opposite sides can accommodate cellular deformations without elongating [green curves in Fig. 2(b)]. By remaining slack [green arrowheads in Figs. 2(b) and 2(c)], these filaments do not contribute to the emergent mechanical response.

For $\mathcal{E} \approx 0.4$, the networks develop several tight tangles connecting taut filaments, Video S5 [33]. This topological reorganization enables sustained cellular stiffening, blue curve in Fig. 2(a). However, the filament strain distribution is extremely broad, indicating that some are strongly elongated while others remain slack, blue arrowheads in Figs. 2(b) and 2(c).

For $\mathcal{E} \gtrsim 0.5$, the networks robustly reorganize into star-shaped configurations (Videos S2 and S6 [33]), mobilizing all filaments with similar elongation, Fig. 2(b), and stiffening beyond an activation strain ε_c^A, Fig. 2(a). We infer that entanglement enables self-organization of the networks into structurally optimal filament arrangements, akin to IF reorganization in superstretched epithelial cells [4], Fig. 1(a). The transition of system behavior beyond a critical degree of entanglement can be interpreted as a
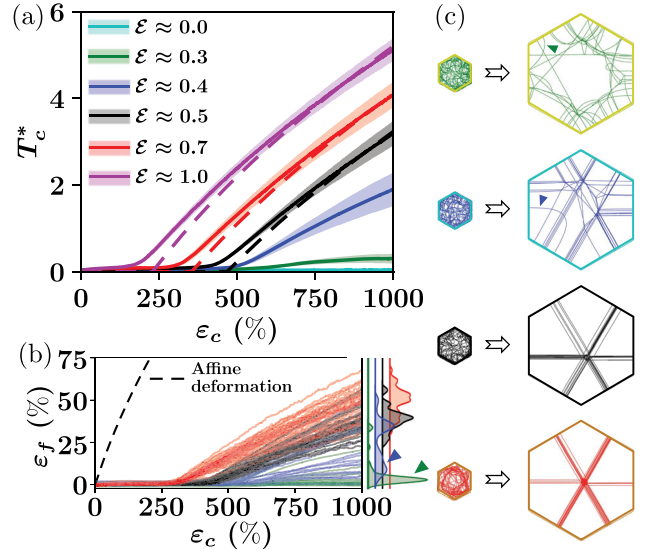
FIG. 2. Influence of filament entanglement on cellular mechanical response. (a) Relation between normalized cellular tension T_c^* and cell areal strain ε_c (solid lines and shadings, mean $\pm$ standard deviation of eight model realizations; dashed lines, 1D analytical model with $\gamma = 1.0, 2.2, 2.9$ for $\mathcal{E} \approx 0.5, 0.7, 1.0$). (b) Evolution of individual filament strain ε_f as a function of cell areal strain for representative realizations of different levels of entanglement and corresponding distributions of filament strain at $\varepsilon_c = 1000\%$ (right shaded curves). The dashed line is the prediction $\varepsilon_f = \sqrt{\varepsilon_c + 1} - 1$ under the assumption of affinity. (c) Representative network reorganizations for $\varepsilon_c = 1000\%$.

topological threshold for mechanical self-organization. Importantly, thanks to their strong nonaffinity, these structurally optimal networks offer mechanical resistance to extreme cell deformations with moderate individual filament strains, defined as $\varepsilon_f = \ell/\ell_0 - 1$ with ℓ the current filament length, Fig. 2(b). For instance, for $\mathcal{E} \approx 0.5$, cell areal strains of $\varepsilon_c = 1000\%$ are accommodated by filament strains of about $\varepsilon_f = 40\%$, much lower than the filament strains around 230% of an equally stretched affine network.

To understand the parameters controlling ε_c^A and the subsequent tension-strain relation, we developed an analytical model assuming network entanglement above the topological threshold, Sec. S6 in the Supplemental Material [33]. Considering the star-shaped geometry of the stretched network and accounting for the filament length stored in the central tight tangle, this model links cell- and filament-scale deformations to estimate the cellular activation strain,

$$\varepsilon_c^A \approx \frac{1}{4a_0^2} \left[\ell_0 - \frac{\pi}{4} \phi \gamma(\mathcal{E}) \mathcal{E}(N_f - 1) \right]^2 - 1, \qquad (3)$$

where $\gamma(\mathcal{E})$ is a phenomenological scalar quantifying the average complexity of individual windings within the central tight tangle. $\gamma = 1$ models a situation in which windings involve filament pairs. With increasing entanglement, we expect windings to involve more filaments and
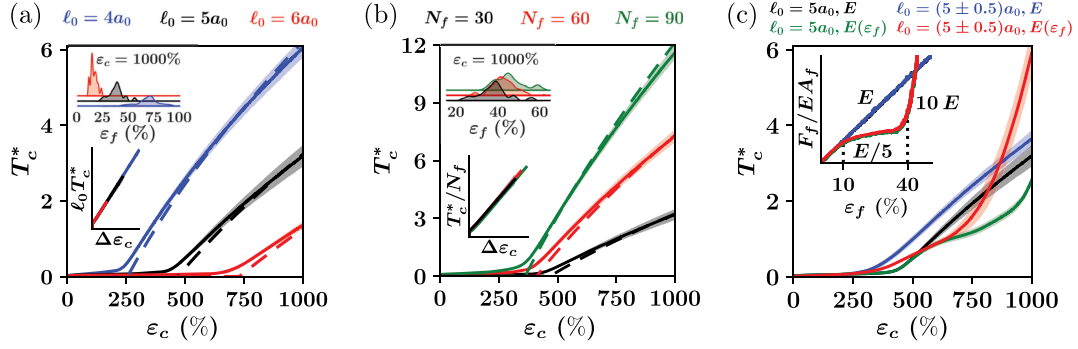
FIG. 3. Cellular mechanical response (solid lines and shadings, mean $\pm$ standard deviation of eight model realizations; dashed lines, 1D analytical model with $\gamma = 1$; insets, $\Delta\varepsilon_c = \langle \sqrt{\varepsilon_c + 1} - \sqrt{\varepsilon_c^A + 1} \rangle$) and filament strain distribution at $\varepsilon_c = 1000\%$ when varying ℓ_0 (a), N_f (b), the distribution of filament lengths ℓ_0, and the filament strain-force relation (c). In all cases, $\mathcal{E} \approx 0.5$.

hence require more length, leading to larger γ. Neglecting filament bending, our model also provides an approximate expression for the dimensionless nominal cellular tension,

$$T_c^* \approx \frac{2N_f a_0}{\ell_0 N_e \tan(\pi/N_e)} \left\langle \sqrt{\varepsilon_c + 1} - \sqrt{\varepsilon_c^A + 1} \right\rangle, \quad (4)$$

where the angle brackets of a real number a are defined by $\langle a \rangle = 0$ if $a < 0$ and $\langle a \rangle = a$ otherwise. Thus, the only fitting parameter is $\gamma(\mathcal{E})$, which should be close to 1 for networks barely above the topological threshold and increase with $\mathcal{E}$, Sec. S6 in [33].

We found a nearly quantitative match between the analytical model with $\gamma = 1$ and simulations at the threshold $\mathcal{E} \approx 0.5$. For higher entanglement, we found very good agreement by increasing γ to 2.2 and 2.9 for $\mathcal{E} \approx 0.7$ and $\mathcal{E} \approx 1.0$, Fig. 2(a), consistent with the idea that networks with larger $\mathcal{E}$ involve windings of increasing complexity. In agreement with our analytical model, the mechanical response of the system above the topological threshold, particularly the emergent stiffness $\partial T_c^*/\partial\varepsilon_c$, is essentially independent of entanglement except for the shift in ε_c^A. Accordingly, we considered a default entanglement $\mathcal{E} \approx 0.5$ in subsequent simulations and set $\gamma = 1$ for the theoretical fits.

According to our theory, as more filament length is stored in the central tight tangle, less length is available for the bundles to bridge cell boundaries. As a result, increasing entanglement should not only increase ε_c^A, but also individual filament strain ε_f for a given cellular strain, in agreement with our simulations [black and red curves in Fig. 2(b)]. Additional simulations show that the mechanical response and network mechanisms described here are not modified by thermal vibrations, Sec. S8 in [33], or changes in filament bending rigidity, Sec. S9 in [33], and that the emergent stiffness scales proportionally to the filament elastic modulus, Sec. S10 in [33].

To further test our theory, we examined the role of filament length, which according to Eqs. (3) and (4), should

modify the activation strain ε_c^A and the emergent tension T_c^*. In agreement with the analytical predictions, simulations with shorter (longer) filaments lead to smaller (larger) activation strains and stiffer (softer) networks, Fig. 3(a), with a marked downward shift in filament strain distributions for longer filaments as more filament length is available to accommodate cellular strain. Per Eq. (4), the tension-strain curves of networks with different filament lengths collapse when representing $\ell_0 T_c^*$ as a function of $\sqrt{\varepsilon_c + 1} - \sqrt{\varepsilon_c^A + 1}$, Fig. 3(a) inset, reflecting the increased compliance of longer filaments. Varying the number of filaments N_f linearly affects the slope of the cellular response, Fig. 3(b), in agreement with Eq. (4). Instead, the number of filaments mildly impacts the activation strain, Fig. 3(b). Thus, filament loading in our entangled networks is determined primarily by $\mathcal{E}$ and ℓ_0, and only weakly by N_f, whereas emergent tension and stiffness are directly controlled by N_f and ℓ_0.

Since IFs exhibit a highly nonlinear force-stretch relation, we then wondered whether the filament constitutive behavior affected the slack-taut transition and the emergent mechanics. We considered filaments that soften to $E/5$ for ε_f in the range between 10% and 40% and eventually restiffen to reach $10E$, mimicking their typical superelastic response [17–22]. The emergent stiffness of the taut network mirrors the individual IF constitutive relations, Fig. 3(c), consistent with the narrow filament strain distributions observed for $\mathcal{E} \gtrsim 0.5$, Fig. 2(b). To examine the influence of filament length variability, we sampled ℓ_0 from a normal distribution with mean $5a_0$ and standard deviation $0.5a_0$. For linearly elastic filaments, this reduces the activation strain, as shorter filaments are mobilized earlier. For nonlinear filaments, the plateau in the filament response is lost at the cellular scale, as the emergent behavior now results from convolving the nonlinear constitutive laws of unequally strained filaments. Cell-scale stiffening is also reached earlier when including shorter filaments. However, the slack-taut transition corresponding to the formation of radial IF bundles remains unchanged,

$N_e = 3$ $N_e = 4$ $N_e = 6$
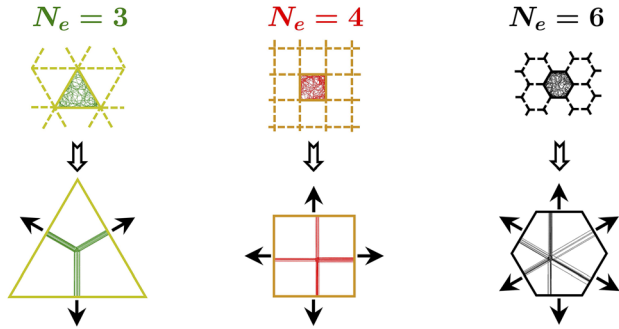
FIG. 4. Network reorganization for different shapes of the enclosing cell, corresponding to regular tessellations of the plane.

Sec. S11 in the Supplemental Material [33]. Thus, while the shape of the emergent mechanical response past the activation strain depends on the constitutive behavior, the number, and the length distribution of the filaments, their nonaffine self-organization into a star-shaped configuration is solely determined by network entanglement.

Following this rationale, the slack-taut transition should also be preserved when varying the cell shape. To test this, we prepared networks with default parameters and enclosed them in cells with the same a_0, but different N_e. According to the three regular tessellations of the plane [54], we compared triangular, square, and hexagonal cells ($N_e = 3, 4, 6$). Remarkably, the nonaffine and nonlinear mechanical response above the topological threshold is independent of cell shape and well described by Eqs. (3) and (4), Fig. 4 and Sec. S12 in [33].

In summary, inspired by the phenomenology of IF networks in epithelial monolayers under stretch [4], we have studied the physical principles supporting the nonlinear and nonaffine mechanical response of an ensemble of entangled extensible filaments confined to a cell with laterally moving boundary attachments. We identify a metric of entanglement $\mathcal{E}$, which robustly predicts a threshold for mechanical activation of all filaments, $\mathcal{E} \gtrsim 0.5$, leading to self-organization of random filament networks into structurally optimal configurations beyond an activation strain. The occurrence of the transition is purely topological, whereas the emergent mechanics depend on length, number, and constitutive response of the filaments, enabling independent control of activation strain and stiffness.

Our work suggests that, through entanglement and self-organization, IF networks provide a safety net for cells against extreme strains. Being rooted in network topology, this emergent material property is complementary to the role of IFs as a safety belt against fast strain rates, which hinges on rate-dependent mechanics of filaments and bundles [21]. Beyond the biological context, network entanglement has been leveraged to enhance the mechanical properties of hydrogels [55,56] and is at the core of textile materials [57–59]. Here, we identify "corralled entanglement" as a scale-free principle for extremely deformable bioinspired materials whose organization lies between random networks and woven materials. By relying on self-organization, this principle is devoid of the synthesis challenges of weaving or knitting at a molecular scale [60].

[*]marco.pensalfini@upc.edu
[†]marino.arroyo@upc.edu

[1] F. Bosveld, I. Bonnet, B. Guirao, S. Tlili, Z. Wang, A. Petitalot, R. Marchand, P.-L. Bardet, P. Marcq, F. Graner, and Y. Bellaïche, Mechanical control of morphogenesis by fat/dachsous/four-jointed planar cell polarity pathway, Science **336**, 724 (2012).

[2] B. Alberts, J. Wilson, and T. Hunt, *Molecular Biology of the Cell*, 6th ed. (Garland Science, New York, 2014).

[3] B. He, K. Doubrovinski, O. Polyakov, and E. Wieschaus, Apical constriction drives tissue-scale hydrodynamic flow to mediate cell elongation, Nature (London) **508**, 392 (2014).

[4] E. Latorre, S. Kale, L. Casares, M. Gómez-González, M. Uroz, L. Valon, R. V. Nair, E. Garreta, N. Montserrat, A. del Campo, B. Ladoux, M. Arroyo, and X. Trepat, Active superelasticity in three-dimensional epithelia of controlled shape, Nature (London) **563**, 203 (2018).

[5] E. Lazarides, Intermediate filaments as mechanical integrators of cellular space, Nature (London) **283**, 249 (1980).

[6] H. Herrmann, H. Bär, L. Kreplak, S. V. Strelkov, and U. Aebi, Intermediate filaments: From cell architecture to nanomechanics, Nat. Rev. Mol. Cell Biol. **8**, 562 (2007).

[7] A. R. Harris, L. Peter, J. Bellis, B. Baum, A. J. Kabla, and G. T. Charras, Characterizing the mechanics of cultured cell monolayers, Proc. Natl. Acad. Sci. U.S.A. **109**, 16449 (2012).

[8] N. Efimova and T. M. Svitkina, Branched actin networks push against each other at adherens junctions to maintain cell–cell adhesion, J. Cell Biol. **217**, 1827 (2018).

[9] F. Huber, A. Boire, M. P. López, and G. H. Koenderink, Cytoskeletal crosstalk: When three different personalities team up, Curr. Opin. Cell Biol. **32**, 39 (2015).

[10] A. Ndiaye, G. Koenderink, and M. Shemesh, Intermediate filaments in cellular mechanoresponsiveness: Mediating cytoskeletal crosstalk from membrane to nucleus and back, Front. Cell Dev. Biol. **10**, 882037 (2022).

[11] L. Chang and R. D. Goldman, Intermediate filaments mediate cytoskeletal crosstalk, Nat. Rev. Mol. Cell Biol. **5**, 601 (2004).

[12] T.-H. Chang, H.-D. Huang, W.-K. Ong, Y.-J. Fu, O. K. Lee, S. Chien, and J. H. Ho, The effects of actin cytoskeleton perturbation on keratin intermediate filament formation in mesenchymal stem/stromal cells, Biomaterials **35,** 3934 (2014).

[13] O. Chaudhuri, S. H. Parekh, and D. A. Fletcher, Reversible stress softening of actin networks, Nature (London) **445,** 295 (2007).

[14] P. A. Janmey, U. Euteneuer, P. Traub, and M. Schliwa, Viscoelastic properties of vimentin compared with other filamentous biopolymer networks, J. Cell Biol. **113,** 155 (1991).

[15] C. P. Broedersz and F. C. MacKintosh, Modeling semiflexible polymer networks, Rev. Mod. Phys. **86,** 995 (2014).

[16] O. I. Wagner, S. Rammensee, N. Korde, Q. Wen, J.-F. Leterrier, and P. A. Janmey, Softness, strength and self-repair in intermediate filament networks, Exp. Cell Res. **313,** 2228 (2007).

[17] L. Kreplak, H. Bär, J. Leterrier, H. Herrmann, and U. Aebi, Exploring the mechanical behavior of single intermediate filaments, J. Mol. Biol. **354,** 569 (2005).

[18] L. Kreplak, H. Herrmann, and U. Aebi, Tensile properties of single desmin intermediate filaments, Biophys. J. **94,** 2790 (2008).

[19] Z. Qin, L. Kreplak, and M. J. Buehler, Hierarchical structure controls nanomechanical properties of vimentin intermediate filaments, PLoS One **4,** e7294 (2009).

[20] Z. Qin and M. J. Buehler, Flaw tolerance of nuclear intermediate filament lamina under extreme mechanical deformation, ACS Nano **5,** 3034 (2011).

[21] J. Block, H. Witt, A. Candelli, E. J. G. Peterman, G. J. L. Wuite, A. Janshoff, and S. Köster, Nonlinear Loading-Rate-Dependent Force Response of Individual Vimentin Intermediate Filaments to Applied Strain, Phys. Rev. Lett. **118,** 048101 (2017).

[22] A. Torres-Sánchez, J. M. Vanegas, P. K. Purohit, and M. Arroyo, Combined molecular/continuum modeling reveals the role of friction during fast unfolding of coiled-coil proteins, Soft Matter **15,** 4961 (2019).

[23] N. Khalilgharibi, J. Fouchard, N. Asadipour, R. Barrientos, M. Duda, A. Bonfanti, A. Yonis, A. Harris, P. Mosaffa, Y. Fujita, A. Kabla, Y. Mao, B. Baum, J. Muñoz, M. Miodownik, and G. Charras, Stress relaxation in epithelial monolayers is controlled by the actomyosin cortex, Nat. Phys. **15,** 839 (2019).

[24] J. Block, V. Schroeder, P. Pawelzyk, N. Willenbacher, and S. Köster, Physical properties of cytoplasmic intermediate filaments, Biochim. Biophys. Acta, Mol. Cell Res. **1853,** 3053 (2015).

[25] N. Wang and D. Stamenovic, Mechanics of vimentin intermediate filaments, J. Muscle Res. Cell Motil. **23,** 535 (2002).

[26] D. Fudge, D. Russell, D. Beriault, W. Moore, E. B. Lane, and A. W. Vogl, The intermediate filament network in cultured human keratinocytes is remarkably extensible and resilient, PLoS One **3,** e2327 (2008).

[27] T. Golde, C. Huster, M. Glaser, T. Händler, H. Herrmann, J. A. Käs, and J. Schnauß, Glassy dynamics in composite biopolymer networks, Soft Matter **14,** 7970 (2018).

[28] J. Duque, A. Bonfanti, J. Fouchard, E. Ferber, A. Harris, A. J. Kabla, and G. T. Charras, Fracture in living cell monolayers, bioRxiv, 10.1101/2023.01.05.522736 (2023).

[29] C. Lorenz, J. Forsting, A. V. Schepers, J. Kraxner, S. Bauch, H. Witt, S. Klumpp, and S. Köster, Lateral Subunit Coupling Determines Intermediate Filament Mechanics, Phys. Rev. Lett. **123,** 188102 (2019).

[30] F. Nedelec and D. Foethke, Collective Langevin dynamics of flexible cytoskeletal fibers, New J. Phys. **9,** 427 (2007).

[31] F. Nedelec, CYTOSIM, GitLab Repository, https://gitlab.com/f-nedelec/cytosim (2023).

[32] M. Pensalfini, CYTOSIM—custom version, GitLab Repository, https://gitlab.com/marco-pensalfini/cytosim (2023).

[33] See Supplemental Material at http://link.aps.org/supplemental/10.1103/PhysRevLett.131.058101, which includes Refs. [34–39], for further details on model generation (S1), adopted model parameters (S2), quantification of pairwise linking number in discrete systems (S3), link between network entanglement metrics and emergent mechanics (S4), influence of cell deformation on $\mathcal{E}$ (S5), analytical model development (S6), role of other cytoskeletal structures toward hindering IF reorganization at high strain rates (S7), influence of system temperature (S8), filament bending rigidity (S9), elastic modulus (S10), length distribution and nonlinear constitutive behavior (S11), and enclosing cell shape (S12) on cell-scale mechanics.

[34] C. P. Descovich, D. B. Cortes, S. Ryan, J. Nash, L. Zhang, P. S. Maddox, F. Nedelec, and A. S. Maddox, Cross-linkers both drive and brake cytoskeletal remodeling and furrowing in cytokinesis, Mol. Biol. Cell **29,** 622 (2018).

[35] D. B. Cortes, M. Gordon, F. Nédélec, and A. S. Maddox, Bond type and discretization of nonmuscle myosin II are critical for simulated contractile dynamics, Biophys. J. **118,** 2703 (2020).

[36] J.-F. Nolting, W. Möbius, and S. Köster, Mechanics of individual keratin bundles in living cells, Biophys. J. **107,** 2693 (2014).

[37] S. Yoon and R. E. Leube, Keratin intermediate filaments: Intermediaries of epithelial cell migration, Essays Biochem. **63,** 521 (2019).

[38] D. S. Fudge, K. H. Gardner, V. T. Forsyth, C. Riekel, and J. M. Gosline, The mechanical properties of hydrated intermediate filaments: Insights from hagfish slime threads, Biophys. J. **85,** 2015 (2003).

[39] D. Stamenović and N. Wang, Stress transmission within the cell, Compr. Physiol. **1,** 499 (2011).

[40] Z. Kechagia, P. Sáez, M. Gómez-González, M. Zamarbide, I. Andreu, T. Koorman, A. E. Beedle, P. W. Derksen, X. Trepat, M. Arroyo, and P. Roca-Cusachs, The laminin-keratin link shields the nucleus from mechanical deformation and signalling, bioRxiv, 10.1101/2022.03.01.482474 (2022).

[41] A. Deglincerti, G. F. Croft, L. N. Pietila, M. Zernicka-Goetz, E. D. Siggia, and A. H. Brivanlou, Self-organization of the in vitro attached human embryo, Nature (London) **533,** 251 (2016).

[42] S. F. Edwards, Statistical mechanics with topological constraints: I, Proc. Phys. Soc. London **91,** 513 (1967).

[43] R. Deam and S. F. Edwards, The theory of rubber elasticity, Phil. Trans. R. Soc. A **280,** 317 (1976).

[44] K. Iwata and S. Edwards, New model of polymer entanglement: Localized Gauss integral model. Plateau modulus G_N, topological second virial coefficient a A_2^θ and physical foundation of the tube model, J. Chem. Phys. **90**, 4567 (1989).

[45] R. Everaers, S. K. Sukumaran, G. S. Grest, C. Svaneborg, A. Sivasubramanian, and K. Kremer, Rheology and microscopic topology of entangled polymeric liquids, Science **303**, 823 (2004).

[46] S. Chmutov, S. Duzhin, and J. Mostovoy, *Introduction to Vassiliev Knot Invariants* (Cambridge University Press, Cambridge, England, 2012).

[47] S. Grishanov, M. Tausif, and S. Russell, Characterisation of fibre entanglement in nonwoven fabrics based on knot theory, Compos. Sci. Technol. **72**, 1331 (2012).

[48] D. W. Sumners, C. Ernst, S. J. Spengler, and N. R. Cozzarelli, Analysis of the mechanism of dna recombination using tangles, Q. Rev. Biophys. **28**, 253 (1995).

[49] J. F. Marko, Biophysics of protein–DNA interactions and chromosome organization, Physica (Amsterdam) **418A**, 126 (2015).

[50] W. Niemyska, K. C. Millett, and J. I. Sulkowska, GLN: A method to reveal unique properties of lasso type topology in proteins, Sci. Rep. **10**, 1 (2020).

[51] R. L. Ricca and B. Nipoti, Gauss' linking number revisited, J. Knot Theory Ramifications **20**, 1325 (2011).

[52] S. Grishanov, V. Meshkov, and A. Omelchenko, A topological study of textile structures. Part II: Topological invariants in application to textile structures, Text. Res. J **79**, 822 (2009).

[53] V. Negi and R. C. Picu, Tensile behavior of non-crosslinked networks of athermal fibers in the presence of entanglements and friction, Soft Matter **17**, 10186 (2021).

[54] B. Grünbaum and G. C. Shephard, Tilings by regular polygons, Math. Mag. **50**, 227 (1977).

[55] J. Kim, G. Zhang, M. Shi, and Z. Suo, Fracture, fatigue, and friction of polymers in which entanglements greatly outnumber cross-links, Science **374**, 212 (2021).

[56] C. Liu, N. Morimoto, L. Jiang, S. Kawahara, T. Noritomi, H. Yokoyama, K. Mayumi, and K. Ito, Tough hydrogels with rapid self-reinforcement, Science **372**, 1078 (2021).

[57] S.-Y. Jeon, W.-J. Na, Y.-O. Choi, M.-G. Lee, H.-E. Kim, and W.-R. Yu, In situ monitoring of structural changes in nonwoven mats under tensile loading using x-ray computer tomography, Compos. Part A-Appl. S. **63**, 1 (2014).

[58] D. Moyo, R. D. Anandjiwala, and A. Patnaik, Micromechanics of hydroentangled nonwoven fabrics, Text. Res. J. **87**, 135 (2017).

[59] D. Liu, S. Koric, and A. Kontsos, A multiscale homogenization approach for architectured knitted textiles, J. Appl. Mech. **86** (2019).

[60] Z.-H. Zhang, B. J. Andreassen, D. P. August, D. A. Leigh, and L. Zhang, Molecular weaving, Nat. Mater. **21**, 275 (2022).